Reduction of the thermal conductivity of the thermoelectric material ScN by Nb alloying

Tureson, Nina; Van Nong, Ngo; Fournier, Daniele; Singh, Niraj ; Acharya, Somnath ; Schmidt, Susann ; Belliard, Laurent ; Soni, Ajay ; Febvrier, Arnaud le ; Eklund, Per

Published in:
Journal of Applied Physics

Link to article, DOI:
10.1063/1.4993913

Publication date:
2017

Document Version
Peer reviewed version

Reduction of the thermal conductivity of the thermoelectric material ScN by Nb alloying

Nina Tureson[1], Ngo Van Nong[2], Daniele Fournier[3], Niraj Singh[4], Somnath Acharya[4], Susann Schmidt[1,5], Laurent Belliard[3], Ajay Soni[4], Arnaud le Febvrier[1]*, Per Eklund[1]*

Affiliations

[1] Department of Physics, Chemistry and Biology (IFM), Linköping University, SE-581 83 Linköping, Sweden

[2] Department of Energy Conversion and Storage, Technical University of Denmark, Risø Campus, Fredriksborgsvej 399, Building 779, 4000 Roskilde, Denmark

[3] Institut des NanoSciences de Paris, Sorbonne Universités, UPMC Universités Paris 06, UMR 7588, Paris F-75005, France

[4] School of Basic Sciences, Indian Institute of Technology Mandi, Mandi, Himachal Pradesh 175001, India

[5] Present address: Ionbond Switzerland – Olten, Coating Center Industriestrasse 211 CH-4600 Olten, Switzerland

*Corresponding authors:

arnaud.le.febvrier@liu.se

per.eklund@liu.se

Keywords:

Nitride, ScN, thin film, sputtering, thermoelectricity, thermal conductivity, alloying

Abstract

ScN-rich (Sc,Nb)N solid solution thin films have been studied motivated by the promising thermoelectric properties of ScN-based materials. Cubic $Sc_{1-x}Nb_xN$ films for $0 \leq x \leq 0.25$ were epitaxially grown by DC reactive magnetron sputtering on c-plane sapphire substrate and oriented along the (111) orientation. The crystal structure, morphology, thermal conductivity, thermoelectric and electrical properties were investigated. The ScN reference film exhibited a Seebeck coefficient of -45μV/K, and a power factor of $6x10^{-4}$ W/mK^2 at 750 K. Estimated from room temperature Hall measurements, all samples exhibit a high carrier density of the order of 10^{21} cm^{-3}. Inclusion of heavy transition metals in ScN enables the reduction the thermal conductivity by an increase of the phonon scattering. The Nb inserted ScN thin films exhibited a thermal conductivity lower than the value of ScN reference (10.5 $Wm^{-1}K^{-1}$) down to a minimum value of 2.2 $Wm^{-1}K^{-1}$. Insertion of Nb into ScN thus yielded to a reduction in thermal conductivity by a factor ~5 due to the mass contrast in ScN which increase the phonon scattering ion the material.

1. Introduction

Transition metal nitrides have recently attracted attention for possible thermoelectric applications, since they possesses outstanding mechanical properties and a broad range of electrical properties.[1-8] Scandium nitride (ScN) is one of them and is an n-type semiconductor with a reported indirect band gap of around 0.9 eV [9,10]. It possesses both a high carrier concentration (10^{18}–10^{22} cm^{-3}), carrier mobility (10-180 cm^2 V^{-1} s^{-1})[9,11] and has a low electrical resistivity of around 300 μΩcm.[1,11] Reported power factors for ScN are relatively high (2.5–3.3 $Wm^{-1}K^{-2}$)[1,2] compared to the common thermoelectric material PbTe.[12] Thus, ScN can be a promising candidate for thermoelectric applications. Numerous techniques have been reported for growth of ScN;[13] a few of them are reactive DC magnetron sputtering [2,9,14], chemical vapor deposition (CVD)[15] and molecular beam epitaxy (MBE).[16] Using DC magnetron sputtering instead of CVD gives the advantages of not using toxic gases and in comparison with MBE; sputtering growth rate is much faster.[17]

The thermoelectric figure of merit (ZT), related to the efficiency of thermoelectric devices is given by $ZT=S^2\sigma T/\kappa$, where S is the Seebeck coefficient, σ is the electrical conductivity and κ is the thermal conductivity. These parameters (S, σ and κ) are all interrelated and there is a need to compromise between these in order to be able to maximize ZT.[18,19] A disadvantage of ScN for thermoelectrics is its relatively high thermal conductivity (8-10 $Wm^{-1}K^{-1}$).[2,20] Several approaches to reduce the thermal conductivity in transition metal nitrides have been suggested like nanoinclusions, doping and superlattices.[21-25] Another proposed approach to reduce the thermal conductivity in ScN thin films is to increase the lattice phonon scattering by alloying ScN with different transition metals. Kerdsongpanya et al.[22] performed first principles calculations of phase stability on a series of possible alloying elements with ScN. One of the suggested alloying elements was niobium for two reasons: (1) the small lattice mismatch

between NbN and ScN and (2) the fact that Nb provides extra electrons to be delocalized in $Sc_{1-x}Nb_xN$. Furthermore, phase stability calculations show negative values of the Gibbs free energy for disordered solid solutions and the presence of Nb is likely to increase the phonon scattering by introducing disturbances in the lattice.[22]

In this work, DC reactive magnetron sputtering have been used to grow Sc-rich $Sc_{1-x}Nb_xN$ films and the effect of Nb insertion on the electronic and thermoelectric properties have been evaluated.

2. Experimental Details

$Sc_{1-x}Nb_xN$ thin films were deposited using DC reactive magnetron sputtering in an ultra-high vacuum chamber (10^{-7} Pa) with Sc and Nb targets (2 inch diameter, MaTek: Sc 99.5%, Nb 99.99%) in an Ar/N_2 (flow ratio 75% Ar / 25% N_2) sputtering-gas mixture. The pressure during depositions was kept at 0.27 Pa (2 mTorr).The chamber is described elsewhere.[26] A maximum total power ($P_{Sc}+P_{Nb}$) of 120W was applied on the sputter and the power of the Nb sputter was gradually increased from 0 to 20 W for each composition. 10 mm x 10 mm one side-polished substrates of Al_2O_3 (c-cut) (Alineason Materials & Technology) were used. The substrates were kept at a temperature of 950^0C and under constant rotation during the deposition. Prior to deposition the substrates was cleaned first in 10 min acetone in ultrasonic bath and then repeated with ethanol and blown dry with a N_2-gun.

X-ray diffraction (XRD) was performed on X'Pert PRO from PANalytical using a Cu K_α radiation with a nickel filter with a Bragg-Brentano configuration (θ-2θ scan) and a 4 circles diffractometer Philips X'Pert-MRD with monochromatic Cu K_α radiation (rocking curves and ϕ scans). The morphology and the cross sections of the films were observed by a scanning

electron microscope (SEM, LEO Gemini 1550, Zeiss). The composition of the $Sc_{1-x}Nb_xN$ films was determined by X-ray photoelectron spectroscopy (XPS) in an Axis Ultra DLD (Kratos Analytical) instrument with a monochromatic AlK_α source.

Thermal conductivity properties of the films was determined by modulated thermoreflectance microscopy (MTRM). In this setup, a pump beam at 532 nm delivered by a Cobolt MLD laser, intensity modulated by an acousto-optical modulator at a frequency f, is focused on the surface of the sample with an objective lens (N.A. = 0.5). In order to prevent effects from possible changes in the optical properties versus the Nb composition, the layers were covered by a 250 nm gold film, this top layer ensuring a heat source located at the surface. Then, thermal waves are excited in the sample and monitored by the reflectivity surface change recorded around the pump location by another focused laser beam. We use a 488 nm Oxius laser to maximize the probe sensitivity to the thermal field in the gold cap layer. A photodiode and a lock-in amplifier record the AC reflectivity component, in a frequency range between 1 kHz and 1 MHz. Finally, the experimental profiles of the amplitude and the phase of the reflected probe beam were fitted according to a standard Fourier diffusion law to extract the thermal conductivity of the films.[27-33]

The in-plane Seebeck coefficient and the electrical resistivity were measured simultaneously under a low-pressure helium atmosphere (~ 0.09 MPa, purity 99.999% with <0.5 ppm residual oxygen) using ULVAC-RIKO ZEM3 from room temperature up to 500 °C. The substrate contribution to the Seebeck coefficient and electrical resistivity is negligible, and the instrumental error is within 7%. The room temperature Hall effect measurements up to 5 T magnetic field were performed employing physical property measurement system (PPMS Dynacool).

3. Results

The composition of the $Sc_{1-x}Nb_xN$ films, as estimated from XPS, is listed in table I. The overall composition for $Sc_{1-x}Nb_xN$ (x=0) is 45.6% scandium, 48.9% nitrogen, 5.0% oxygen, 0.2% carbon and 0.3% fluorine. The sample with x = 0.04 has its Sc, Nb and N ratios varying in comparison with the rest of the sample. This sample contains a lower amount of N and a higher amount of impurities, such as oxygen and carbon. The level of impurities is reduced when introducing more Nb. The metal (Sc+Nb) to nitrogen ratio increases from 0.93 to 1.05 when x increases from 0 to 0.25

Figure 1a shows θ-2θ XRD patterns of ScN on sapphire (0001) substrates. One large peak, the ScN 111 peak, is observed at 34.5 degrees. Figure 1b is a magnified view of the ScN 111 peak. This peak gradually shifts towards higher 2θ angles with increasing Nb content. The 111 peaks presents an asymmetry characteristic of using a non-monochromatic beam ($K\alpha_1$ + $K\alpha_2$). The inset in figure 1b presents the lattice parameters estimated from the 111 peak considering a cubic symmetry in comparison to the ones predicted by the Vegard's law using the values of ScN and NbN taken from the ICDD data base (ICDD PDF 00-045-0978 (ScN) and ICDD PDF 03-065-5011 (NbN)). A difference in the slope between the PDF data and the lattice parameters in this work can be seen, but the trend of the decreasing lattice parameter with increasing x is valid.

In figure 2a, the Full With at Half Maximum (FWHM) values from the XRD rocking curves of the ScN 111 peak are presented. The inset shows the ScN rocking curve. The FWHM value decreases when the Nb content increases. Figure 2b shows a φ-scan of the ScN 111

reflection measured at $\psi = 70.5^0$. Six reflections are present and separated by 60°instead of the three expected in a cubic crystal system, because of the twin domain symmetry when growing ScN on sapphire (0001).[1] Both types of XRD results indicate epitaxial growth of good quality. Figure 3 shows the crystals structure in the (0001) plane of sapphire and in the (111) plane of ScN in both metallic and anion network of the respective crystal network (metallic and anion). The crystal structure of both materials were drawn using a cell parameter from the bulk material (ICDD data file: ICDD PDF 00-045-0978 (ScN) and ICDD PDF 01-071-1684 (Al_2O_3)). An [111] growth direction for the cubic cell of ScN is expected on a c-plane sapphire with an epitaxial-like relationship of $[111]_{ScN}//[0001]_{Al2O3}$ and $[22\bar{1}]_{ScN}//[1000]_{Al2O3}$. In both networks, the epitaxial like growth of ScN on c-plane sapphire would be possible with a compressive stress. The mismatch appeared to be positive and equal to + 14%.

SEM images and the optical appearance of the $Sc_{1-x}Nb_xN$ films series are presented in figure 4. SEM images show fairly smooth films, but in the case of low Nb content, grains with larger grain size (50-100 nm) were observed. The ScN film exhibited a yellowish color. When the Nb content increased in $Sc_{1-x}Nb_xN$, the appearance of the films changes to more brown color. The thicknesses measured from the film cross sections give values between 95 and 130 nm.

Figure 5 displays the thermal conductivity values obtained from the thermoreflectance measurement. A decrease of the thermal conductivity is clearly observed when Nb is introduced into ScN. The thermal conductivity decrease from 11.0 $Wm^{-1}K^{-1}$ to a minimum value of 2.2 $Wm^{-1}K^{-1}$ obtained for x=0.13 which corresponds to 20 % of the ScN thermal conductivity value. Earlier reported thermal conductivity values for ScN are around 10 $Wm^{-1}K^{-1}$.[2,19]

In figure 6, the Seebeck coefficient, electrical resistivity and the corresponding power factor from the simultaneous measurements are presented. The ScN reference sample and the film with a Nb content of x=0.04 exhibited similar Seebeck coefficients with for example values of -42 μV/K at 750 K. However, with further increasing Nb concentration in the ScN, the absolute value of the Seebeck coefficient is reduced to 17 μV/K (750K). The electrical resistivity of the ScN reference thin film is around 300 μΩcm. The insertion of Nb in ScN lead to an increase of resistivity to values between 550 and 800 μΩcm. The samples with x = 0.25 exhibited a lower resistivity values of 550 μΩcm at 750 K. The power factors (S^2/ρ) are the highest for the ScN reference films compared to the Nb-containing films.

The carrier density (n) as a function of Nb content in ScN at room temperature (300 K) is shown in figure 7. All samples exhibit a high carrier density of the order of 10^{21} cm^{-3}. Although, among the Nb-containing films, the carrier concentration increased when x increases from 0.07 to 0.25. Here, n for x = 0.04 does not follow the trend and shows a higher value relative to other samples, in line with the higher amount of disorder and impurities such as oxygen and carbon present in the sample present with a higher amount than the other samples.

4. Discussion

The composition of the $Sc_{1-x}Nb_xN$ thin films varied as expected with the applied target power ratio; the amount of Nb increased while the Sc content is decreased. The nitrogen level in the films (except for x=0.04) indicates that the films were nearly stoichiometric with a metal/nitrogen ratio between 0.93 and 1.05. Earlier reports on ScN growth shows that oxygen and other impurities influences the properties of ScN such as the carrier concentration. [13,34,35] From the XPS results, it is evident that the level of impurities is high. For x=0.04, these levels are particularly high for both oxygen and carbon. The oxygen content in the films was reduced with increasing Nb concentration, but the carbon amount does not show a clear trend. The fluorine present in the film originates from the Sc target and is usually observed .[34] The small difference in metal to nitrogen ratio between the $Sc_{1-x}Nb_xN$ films could possibly be reduced if the amount of the impurities was reduced. The presence of impurities may also result in different amount of N vacancies present in the films which could give shifts in the density of states. [16,34,36]

The single phase $Sc_{1-x}Nb_xN$ thin films were grown epitaxially on c-plane sapphire along its [111] direction as observed on the φ-scan with a $\Delta\varphi$ of 1.6° for ScN thin film. The experimental data showed a decrease of the cell parameter with an increasing Nb content, demonstrating the solid solution of Nb on Sc sites in ScN. The data on evolution of the experimental cell parameter with the Nb content have a small difference in slope and a slight offset in comparison to Vegard's law, which is not surprising for the case of epitaxial growth and the low thickness of the film which may lead to a strained films. The quality of out-of-plane orientation evaluated with the value of the $\Delta\omega$ showed an improvement of the quality of the (111) orientation. This improvement of orientation quality (improvement of epitaxial growth) for the $Sc_{1-x}Nb_xN$ films can be explained by a reduction of the cell volume of the cubic $Sc_{1-x}Nb_xN$ when x increases. The volume of the unit cell decreases slightly because of the mismatch between the

film and the substrate and consequently leading to an improved epitaxial growth. The features visible in the SEM figures for the $Sc_{1-x}Nb_xN$ films (x=0.04, 0.07 & 0.13) probably arise from small differences in the lattice parameters rather than other orientations of the films. Since no other peaks except for the sapphire 0006 and ScN 111 peaks were observed, an discontinuous grain growth of ScN may occurs at defects located on the substrate surface, for example the atomic steps.

From the thermal conductivity measurements, there is a drastic reduction of the thermal conductivity for the $Sc_{1-x}Nb_xN$ thin films with higher amount of Nb with a minimum thermal conductivity corresponding, for example to the 1/5 of the ScN values for the samples with x=0.13. This confirms the prediction by Kerdsongpanya *et al.* [21] that the phonon scattering increases and reduces the thermal lattice conductivity when incorporating Nb in ScN. Already at low Nb content (x = 0.04), the reduction is substantial with a thermal conductivity of around 7 $Wm^{-1}K^{-1}$. Apart from interfaces, grain boundaries, defects, the mass-contrasts in the material plays an important role in attenuation of phonon transport leading to a drastic decrease in the total thermal conductivity of the sample. The large difference in the atomic mass of Sc (44.95 u) and Nb (92.90 u) gives rise to large scale phonon damping. Hence, a significant reduction in thermal conductivity for $Sc_{1-x}Nb_xN$ samples is observed. Given that Sc is isotope-pure,[37] and pure ScN thus lacks natural isotope scattering means that the effect of alloying or doping on thermal conductivity is particularly important for this material.

The Seebeck coefficient and the electrical resistivity for the ScN (x=0) is similar to earlier reported values, but have lower power factor than the top ones.[1,2] The limiting factor of the ScN to get maximum thermoelectric performance is likely its sensitivity to impurities, which results in reduced Seebeck coefficients. Even though a large reduction of the thermal conductivity can be achieved by Nb incorporation, the absolute value of the Seebeck coefficient

is decreased and in the same time the electrical resistivity is increased for higher Nb contents. The increased electrical resistivity of the films can be described with the increased charge-carrier scattering, impurities and defects which may affect the mobility of the charge carriers more than the carrier concentration itself.[36] Thus, while there is a major reduction in thermal conductivity, the purity of the films may need to be improved to reach an overall improvement in thermoelectric properties.

5. Conclusions

Epitaxial $Sc_{1-x}Nb_xN$ thin films were grown by DC reactive magnetron sputtering. Incorporating Nb in ScN lead to a reduced thermal conductivity by a factor ~5 because of phonon scattering with the heavy 4d metal. The ScN film exhibited a moderate Seebeck coefficient of -45μV/K, and a power factor of $6x10^{-4}$ W/mK^2 at 750K. Insertion of Nb into the ScN deteriorates the Seebeck coefficient and the power factor by a factor ~5. The overall thermoelectric properties (ZT) of the $Sc_{1-x}Nb_xN$ thin film would be expected to be similar to the ScN thin film, with power factor and a thermal conductivity both reduced by a factor 5. This study showed the possibility to reduce the thermal conductivity by mass-contrasts in this type of semiconductors.

Acknowledgments

The authors acknowledge funding from the European Research Council under the European Community's Seventh Framework Programme (FP/2007-2013)/ERC grant agreement no. 335383, the Swedish Foundation for Strategic Research (SSF) through the Future Research Leaders 5 program, the Swedish Research Council (VR) under project nos. 621-2012-4430 and

2016-03365, the Knut and Alice Wallenberg Foundation through the Wallenberg Academy Fellows program, and the Swedish Government Strategic Research Area in Materials Science on Functional Materials at Linköping University (Faculty Grant SFO-Mat-LiU No. 2009 00971). N. V. Nong would like to thank the financial support by the projects NanoCaTe (FP7-NMP No. 604647) and CTEC (No. 1305-00002B).

6. References

[1] S. Kerdsongpanya, N. Van Nong, N. Pryds, A. Žukauskaitė, J. Jensen, J. Birch, J. Lu, L. Hultman, G. Wingqvist, and P. Eklund, Applied Physics Letters **99,** 232113 (2011).

[2] P. V. Burmistrova, J. Maassen, T. Favaloro, B. Saha, S. Salamat, Y. Rui Koh, M. S. Lundstrom, A. Shakouri, and T. D. Sands, Journal of Applied Physics **113,** 153704 (2013).

[3] C. X. Quintela, J. P. Podkaminer, C. B. Eom, M. N. Luckyanova, G. Chen, T. R. Paudel, E. Y. Tsymbal, E. L. Thies, D. A. Hillsberry, D. A. Tenne, and F. Rivadulla, Advanced Materials **27,** 3032 (2015).

[4] P. Eklund, S. Kerdsongpanya, and B. Alling, Journal of Materials Chemistry C **4,** 3905 (2016).

[5] A. S. Botana, V. Pardo, and W. E. Pickett, Physical Review B **93,** 085125 (2016).

[6] A. S. Botana, V. Pardo, and W. E. Pickett, Physical Review Applied **7,** 024002 (2017).

[7] O. Jankovský, D. Sedmidubský, Š. Huber, P. Šimek, and Z. Sofer, Journal of the European Ceramic Society **34,** 8 4131 (2014).

[8] C. X. Quintela, F. Rivadulla, and J. Rivas, Applied Physics Letters **94,** 152103 (2009).

[9] J. M. Gregoire, S. D. Kirby, G. E. Scopelianos, F. H. Lee, and R. B. van Dover, Journal of Applied Physics **104,** 074913 (2008).

[10] H. A. Al-Brithen, A. R. Smith, and D. Gall, Physical Review B **70,** 045303 (2004).

[11] B. Saha, M. Garbrecht, J. A. Perez-Taborda, M. H. Fawey, Y. R. Koh, A. Shakouri, M. Martin-Gonzalez, L. Hultman, and T. D. Sands, Applied Physics Letters **110,** 252104 (2017).

[12] J. R. Sootsman, J. He, V. P. Dravid, C.-P. Li, C. Uher, and M. G. Kanatzidis, Journal of Applied Physics **105,** 083718 (2009).

[13] S. W. King, R. F. Davis, and R. J. Nemanich, Journal of Vacuum Science & Technology A **32,** 061504 (2014).

[14] D. Gall, I. Petrov, L. D. Madsen, J.-E. Sundgren, and J. E. Greene, Journal of Vacuum Science & Technology A **16,** 2411 (1998).

[15] Z. Gu, J. H. Edgar, J. Pomeroy, M. Kuball, and D. W. Coffey, Journal of Materials Science: Materials in Electronics **15,** 555 (2004).

[16] A. R. Smith, H. A. H. Al-Brithen, D. C. Ingram, and D. Gall, Journal of Applied Physics **90,** 1809 (2001).

[17] D. M. Mattox, Handbook of Physical Vapor Deposition (PVD) Processing (Elsevier Inc., 2010).

[18] G. J. Snyder and E. S. Toberer, Nat Mater **7,** 105 (2008).

[19] J. R. Sootsman, D. Y. Chung, and M. G. Kanatzidis, Angewandte Chemie International Edition **48,** 8616 (2009).

[20] V. Rawat, Y. K. Koh, D. G. Cahill, and T. D. Sands, Journal of Applied Physics **105,** 024909 (2009).

[21] B. Saha, T. D. Sands, and U. V. Waghmare, Journal of Applied Physics **109,** 083717 (2011).

[22] S. Kerdsongpanya, B. Alling, and P. Eklund, Journal of Applied Physics **114,** 073512 (2013).

[23] S. Kerdsongpanya, B. Sun, F. Eriksson, J. Jensen, J. Lu, Y. K. Koh, N. V. Nong, B. Balke, B. Alling, and P. Eklund, Journal of Applied Physics **120,** 215103 (2016).
[24] J. L. Schroeder, D. A. Ewoldt, R. Amatya, R. J. Ram, A. Shakouri, T. D. Sands, Journal of microelectromechanical systems **23,** 672 (2014).
[25] C. X. Quintela, B. Rodríguez-González, and F. Rivadulla, Applied Physics Letters **104,** 022103 (2014).D.H.
[26] Trinh, H.Hogberg, J. M. Andersson, M. Collin, I. Reineck, U.Helmersson, andL. Hutman, Journal of Vacuum Sciences and Technology A **24,** 309 (206)
[27] L. Pottier, Appl. Phys. Lett. **64**, 1618 (1994)
[28] B. Li, J.-P. Roger, L. Pottier, D. Fournier, Journal of Applied Physics **86**, 5314 (1999)
[29] K. Plamann, D. Fournier, B.C. Forget, A.C. Boccara, Diamond and Related Materials **5**, 699 (1996)
[30] C. Frétigny, J.P. Roger, V. Reita and D. Fournier Journal of Applied Physics **102**, 116104, (2007)
[31] C. Frétigny, J-Y Duquesne, D. Fournier and F. Xu, Journal of Applied Physics **111**, 084313 (2012)
[32] F. Xu, C. Frétigny, D. Fournier, L. Belliard, S. Vincent, B. Perrin, S. Martin, C. Secouard and J.-Y. Duquesne, Journal of Applied Physics **113**, 244304, (2013)
[33] C. Frétigny, J-Y Duquesne, D. Fournier, International Journal of Thermophysics **5-6,** 1281-1288 (2015)
[34] R. Deng, B. D. Ozsdolay, P. Y. Zheng, S. V. Khare, and D. Gall, Physical Review B **91,** 045104 (2015).
[35] Y. Oshima, E. G. Víllora, and K. Shimamura, Journal of Applied Physics **115,** 153508 (2014).
[36] D. Gall, I. Petrov, and J. E. Greene, Journal of Applied Physics **89,** 401 (2001).
[37] C. Nordling and J. Österman, Physics handbook for science and engineering (Studentlitteratur AB , Lund, Sweden, 2006).

Table 1

x in $Sc_{1-x}Nb_xN$	Sc (2p)	Nb (3d)	N (1s)	O (1s)	C (1s)	F (1s)	Impurities (total)	Ratio Me/N	Thickness (nm)
0	45.6	0	48.9	5.0	0.2	0.3	5.5	0.93	130
0.04	41.0	1.6	42.9	10.8	3.6	0.1	14.5	0.99	105
0.07	42.7	3.1	47.7	5.4	1.0	0.1	6.5	0.96	105
0.13	40.8	6.1	47.3	5.3	0.5	0	5.8	0.99	105
0.18	39.4	8.9	48.4	3.2	0	0.1	3.3	1.00	95
0.25	36.8	12.6	47.2	2.5	0.8	0.1	3.4	1.05	115

Table 1. Composition analysis (%) of the films measured using XPS and calculated on the core-level peaks corresponding to each element detected. The metal/nitrogen (Me/N) ratios and thicknesses are also reported.

Figure captions

Figure 1. a) X-ray diffraction patterns (θ-2θ scan) of $Sc_{1-x}Nb_xN$ grown on sapphire (0001) substrates. The x in $Sc_{1-x}Nb_xN$ is represented with corresponding number and color in the graph. b) Magnified view of the ScN (111) peak. The inset graph shows the calculated lattice parameters in comparison with Vegard's law.

Figure 2. a) FWHM of rocking curve measurements of ScN (111) peaks of the films. The inset shows the rocking curve from the ScN. b) XRD φ-scan of ScN grown on sapphire (0001) measured at tilt angle ψ of 70.5□.

Figure 3. Scheme of the epitaxial relationship between c-plane Al_2O_3 and ScN on the metallic and anion network. The (0001) plane of sapphire is represented by aluminum ions (grey) and oxygen ions (red). The (111) plane of ScN is represented by scandium ions (blue) and nitrogen ions (green).

Figure ***4.*** *The morphology (left)) and optical appearance (right) of the $Sc_{1-x}Nb_xN$ films. The numbers on the left represent the x in $Sc_{1-x}Nb_xN$.*

Figure 5. The thermal conductivity values of the different films at 300 K obtained by fitting of the modulated thermoreflectance microscopy measurements. *Model: 250 nm gold ($k = 225$ W/mK; $D = 0.9\times10^{-4}$ m^2/s) / $Sc_{1-x}Nb_xN$ film on Al_2O_3 ($k = 46$ W/mK; $D = 1.48\times10^{-5}$ m^2/s).*

Figure 6. a) Seebeck coefficient, b) Electrical resistivity, and c) The calculated corresponding power factors for $Sc_{1-x}Nb_xN$ films. The x in $Sc_{1-x}Nb_xN$ is shown via the numbers and their corresponding colors inside the Seebeck coefficient graph. The electrical resistivity and the Seebeck coefficient are measured simultaneously every 50 degrees.

Figure 7. Carrier density 'n' as a function of Nb content in ScN, estimated from Hall measurements.

Figure 1

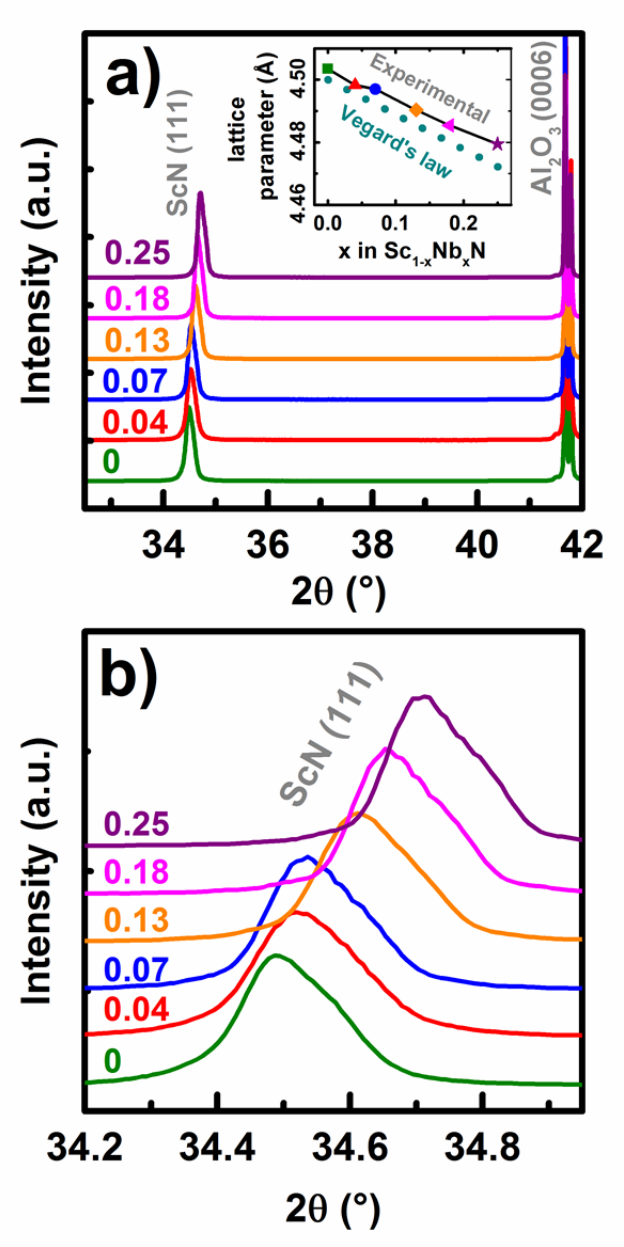
a)
ScN (111)
Al2O3 (0006)
lattice parameter (Å)
4.50
4.48
4.46
0.0
0.1
0.2
x in Sc1-xNbxN
Experimental
Vegard's law
0.25
0.18
0.13
0.07
0.04
0
Intensity (a.u.)
34
36
38
40
42
2θ (°)
b)
ScN (111)
0.25
0.18
0.13
0.07
0.04
0
Intensity (a.u.)
34.2
34.4
34.6
34.8
2θ (°)

Figure 2

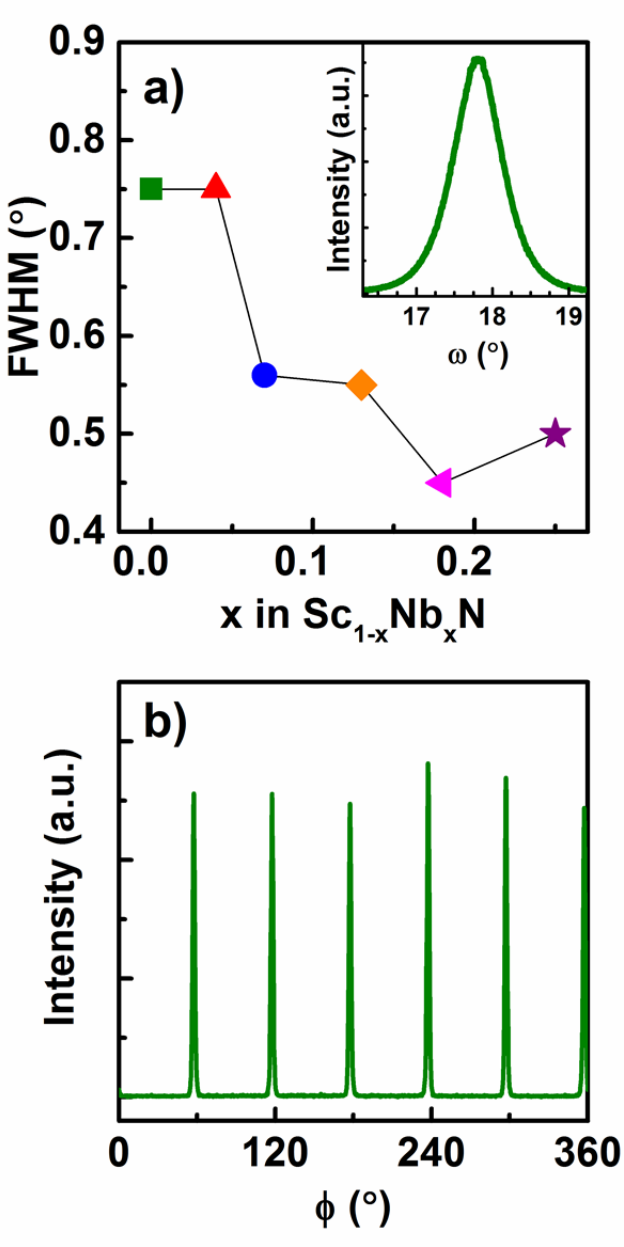
a)
FWHM (°)
0.9
0.8
0.7
0.6
0.5
0.4
0.0
0.1
0.2
x in Sc1-xNbxN
Intensity (a.u.)
17
18
19
ω (°)
b)
Intensity (a.u.)
0
120
240
360
ϕ (°)

Figure 3

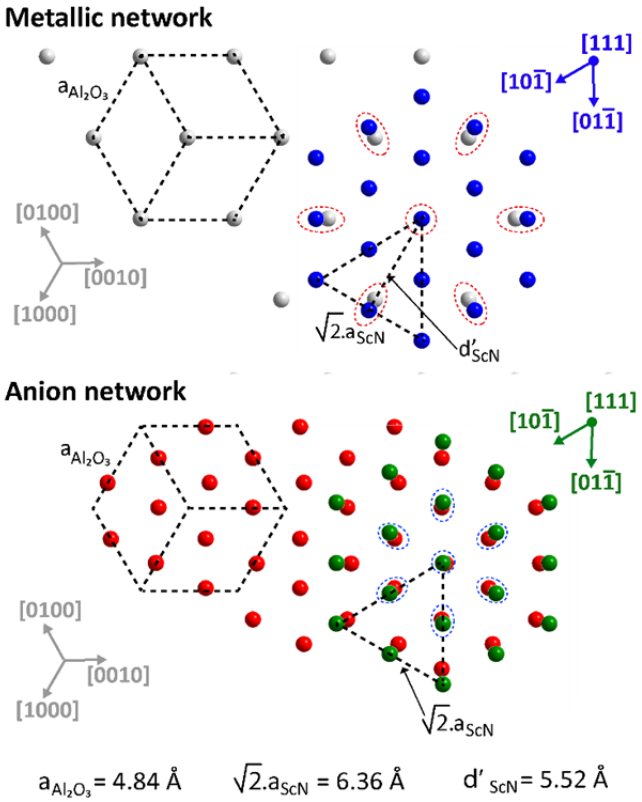

$a_{Al_2O_3}$ = 4.84 Å $\sqrt{2}.a_{ScN}$ = 6.36 Å d'_{ScN} = 5.52 Å

Figure 4

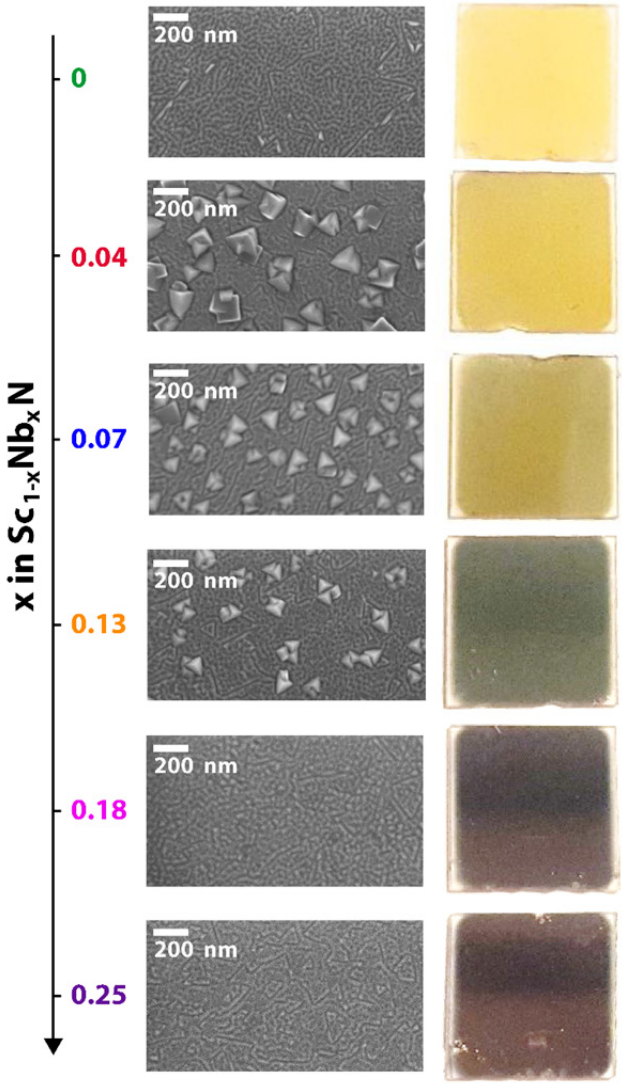
x in $Sc_{1-x}Nb_xN$
0
0.04
0.07
0.13
0.18
0.25
200 nm
200 nm
200 nm
200 nm
200 nm
200 nm

Figure 5

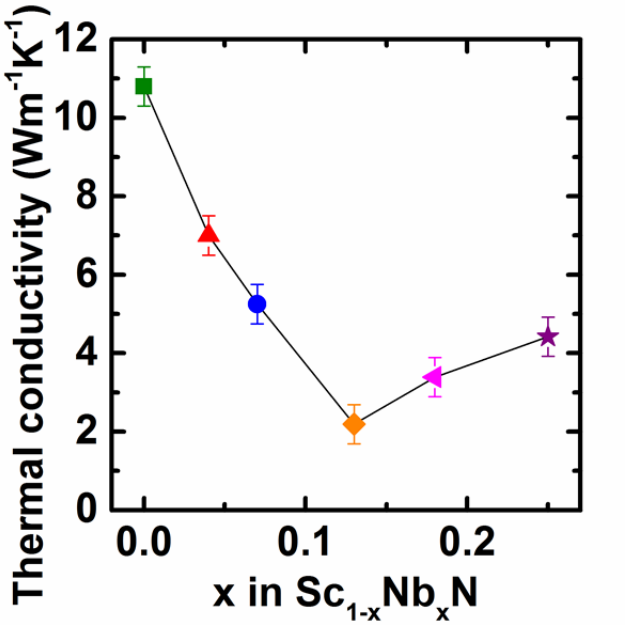
Thermal conductivity (Wm-1K-1)
12
10
8
6
4
2
0
0.0
0.1
0.2
x in Sc1-xNbxN

Figure 6

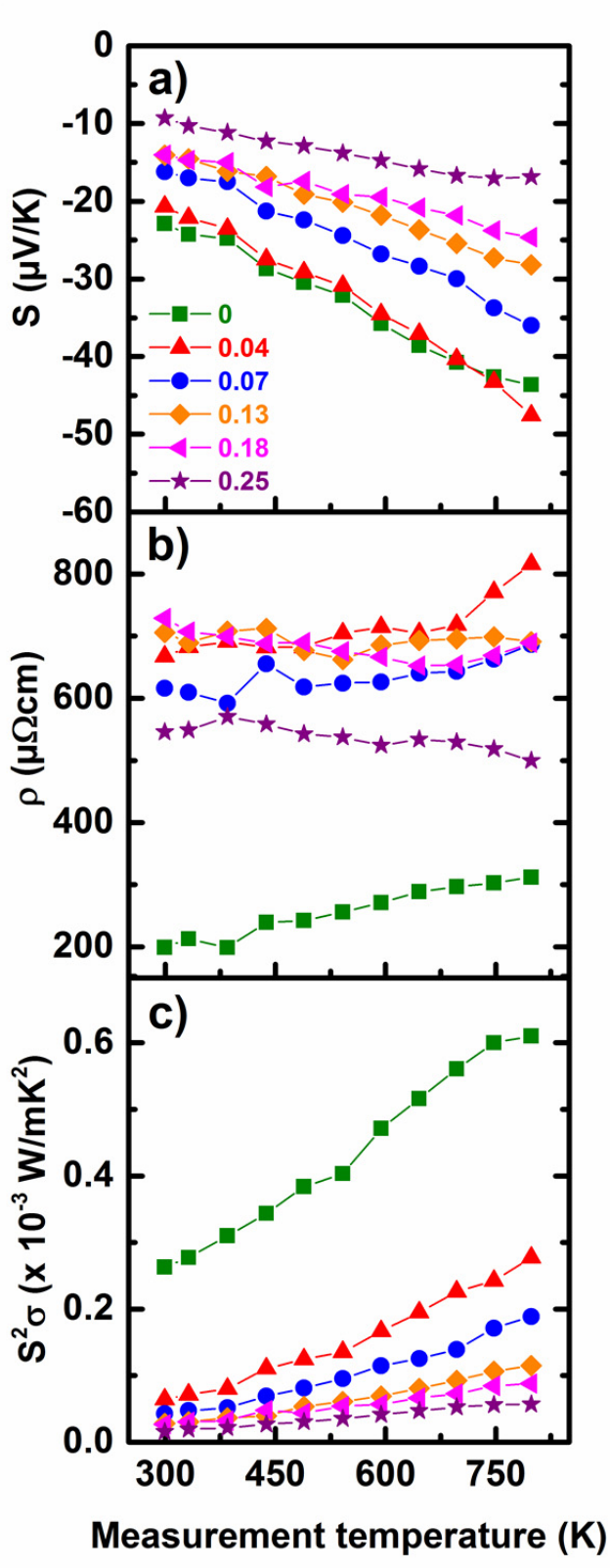
a)
b)
c)
S (μV/K)
ρ (μΩcm)
S²σ (x 10⁻³ W/mK²)
Measurement temperature (K)
0
0.04
0.07
0.13
0.18
0.25

Figure 7

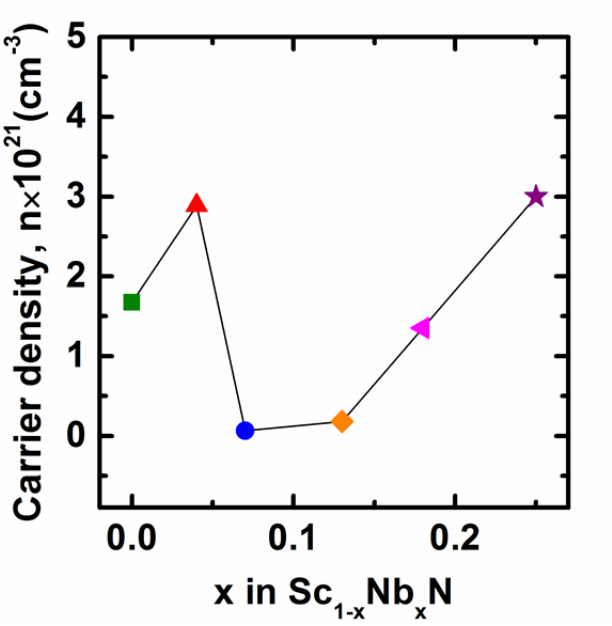

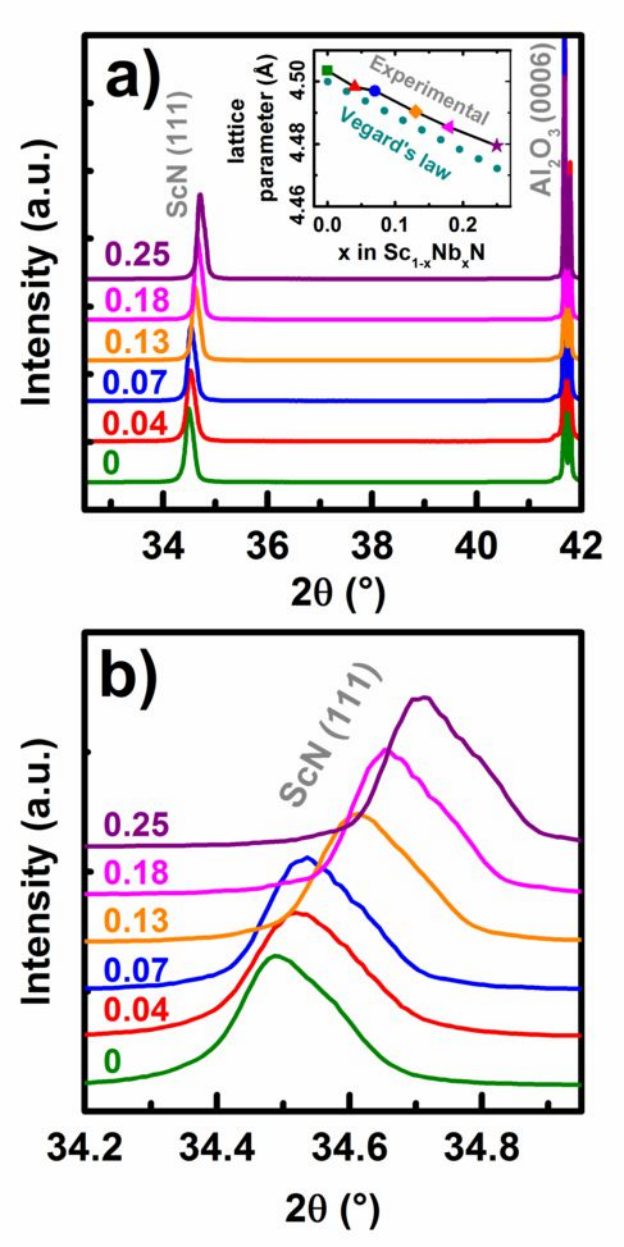
a)
ScN (111)
Al2O3 (0006)
Intensity (a.u.)
0.25
0.18
0.13
0.07
0.04
0
34
36
38
40
42
2θ (°)
lattice parameter (Å)
4.50
4.48
4.46
Experimental
Vegard's law
0.0
0.1
0.2
x in Sc1-xNbxN
b)
ScN (111)
Intensity (a.u.)
0.25
0.18
0.13
0.07
0.04
0
34.2
34.4
34.6
34.8
2θ (°)

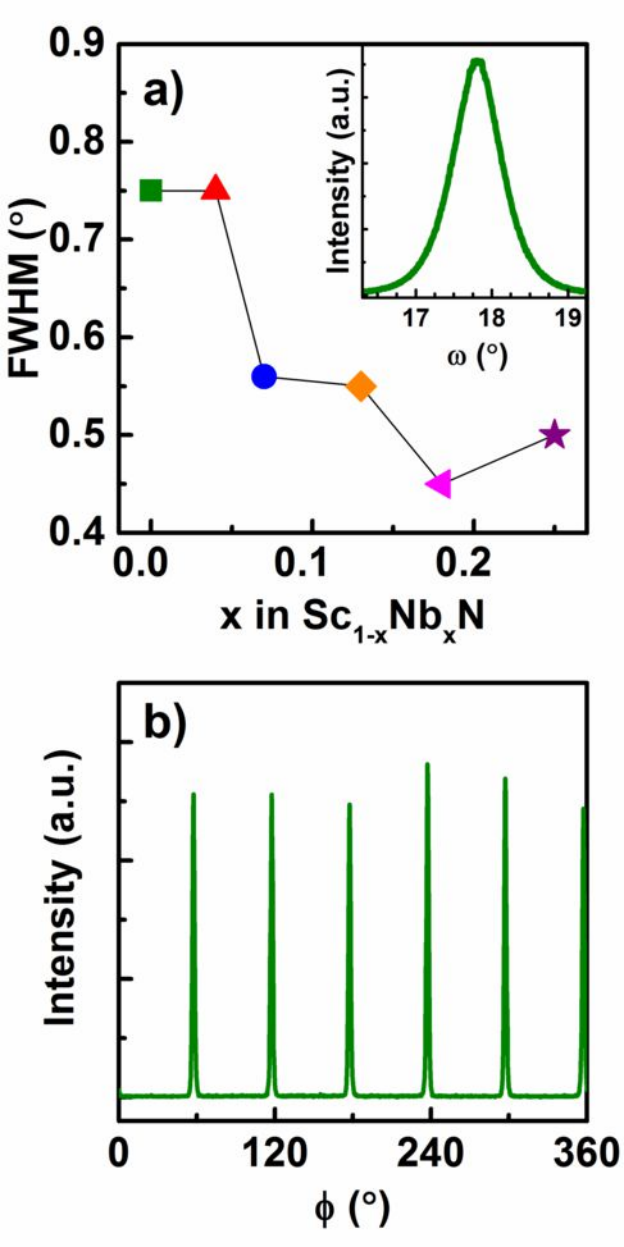
a)
FWHM (°)
0.9
0.8
0.7
0.6
0.5
0.4
0.0
0.1
0.2
x in Sc1-xNbxN
Intensity (a.u.)
17
18
19
ω (°)
b)
Intensity (a.u.)
0
120
240
360
ϕ (°)

Metallic network

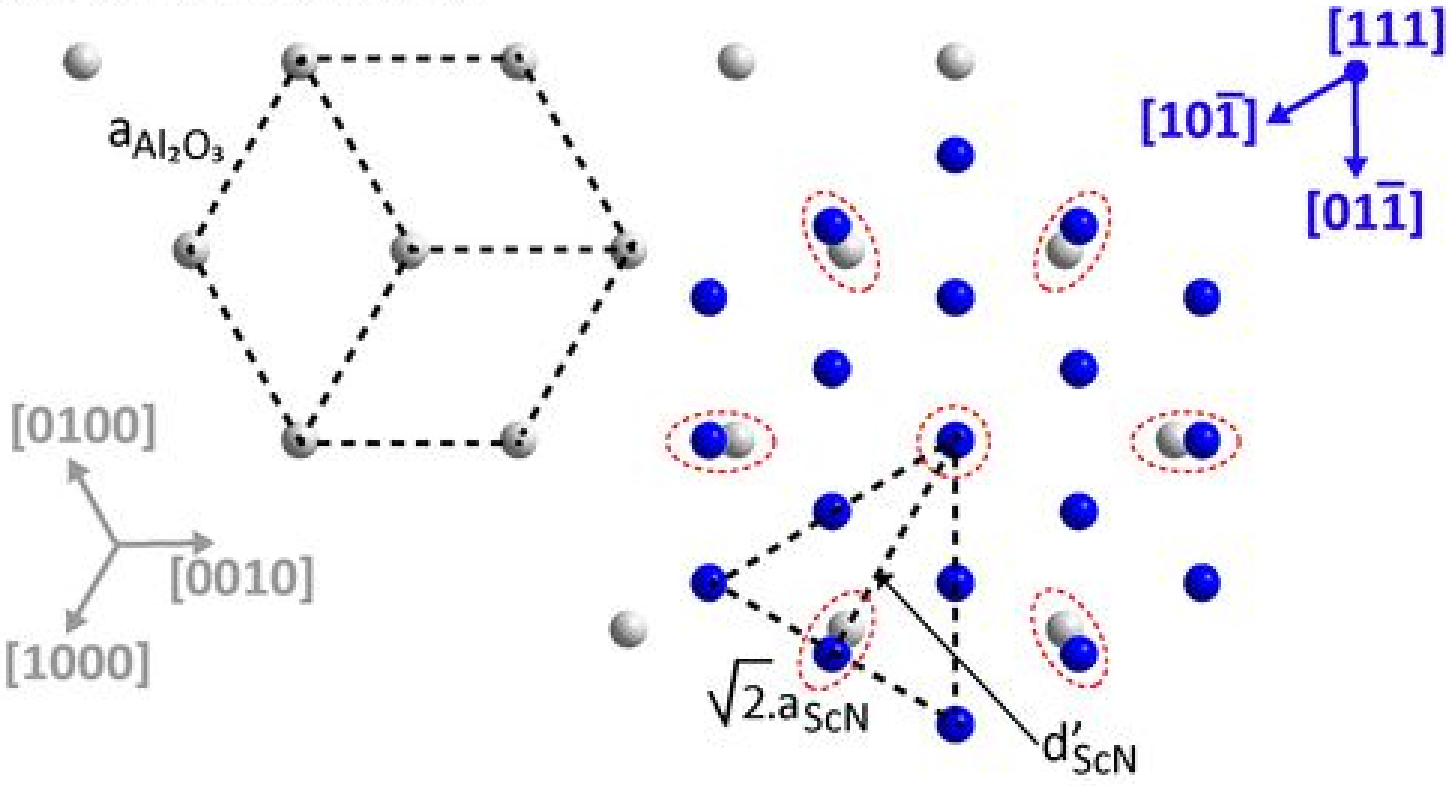

Anion network

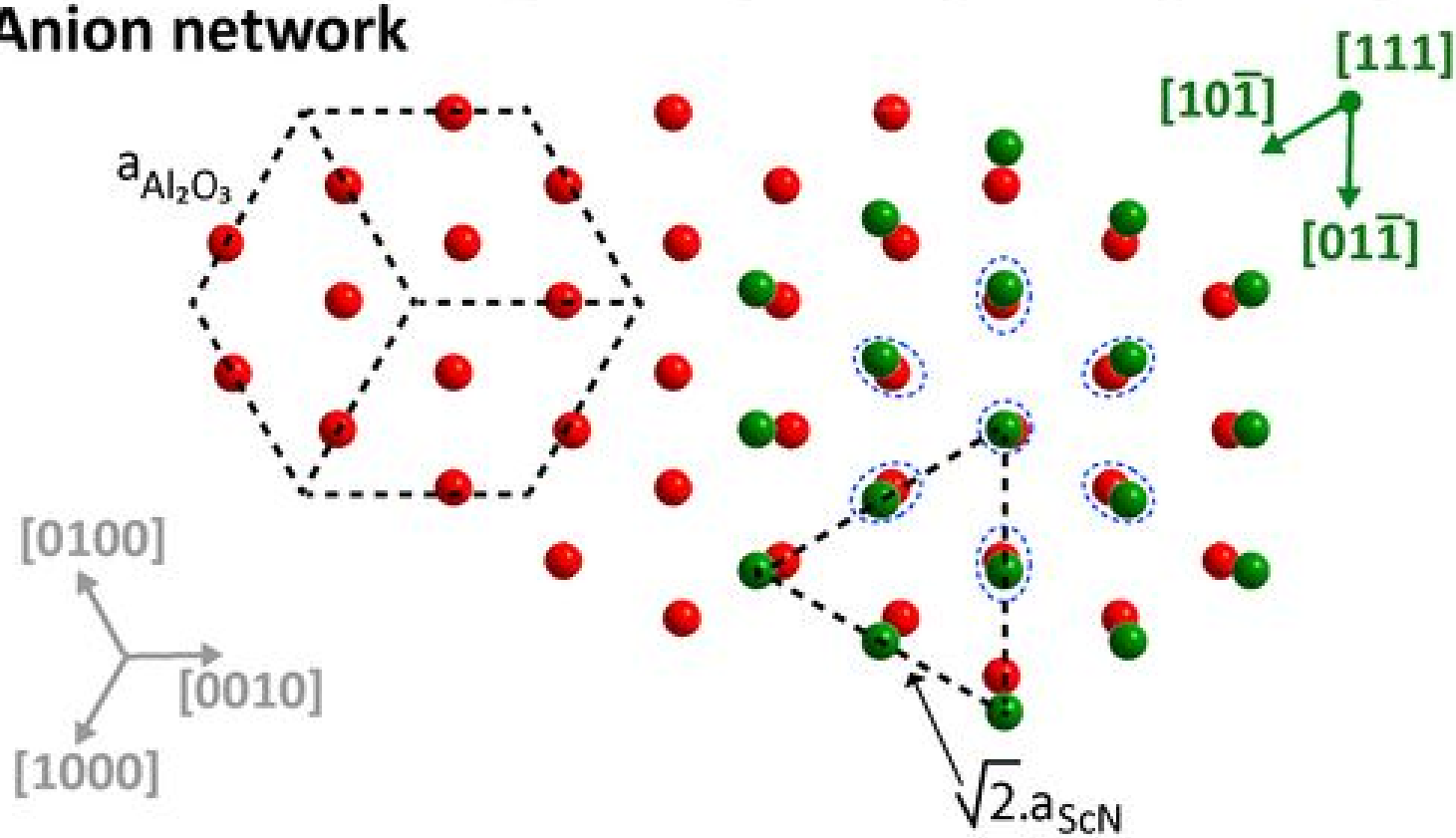

$a_{Al_2O_3}$ = 4.84 Å $\sqrt{2}.a_{ScN}$ = 6.36 Å d'_{ScN} = 5.52 Å

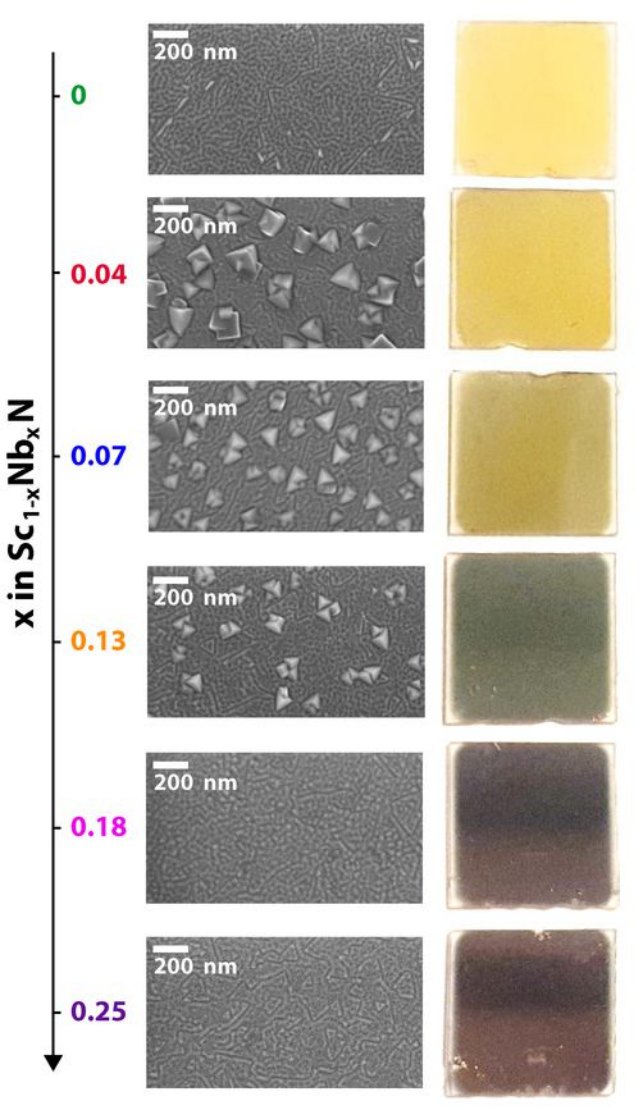
x in $Sc_{1-x}Nb_xN$
0
0.04
0.07
0.13
0.18
0.25
200 nm
200 nm
200 nm
200 nm
200 nm
200 nm

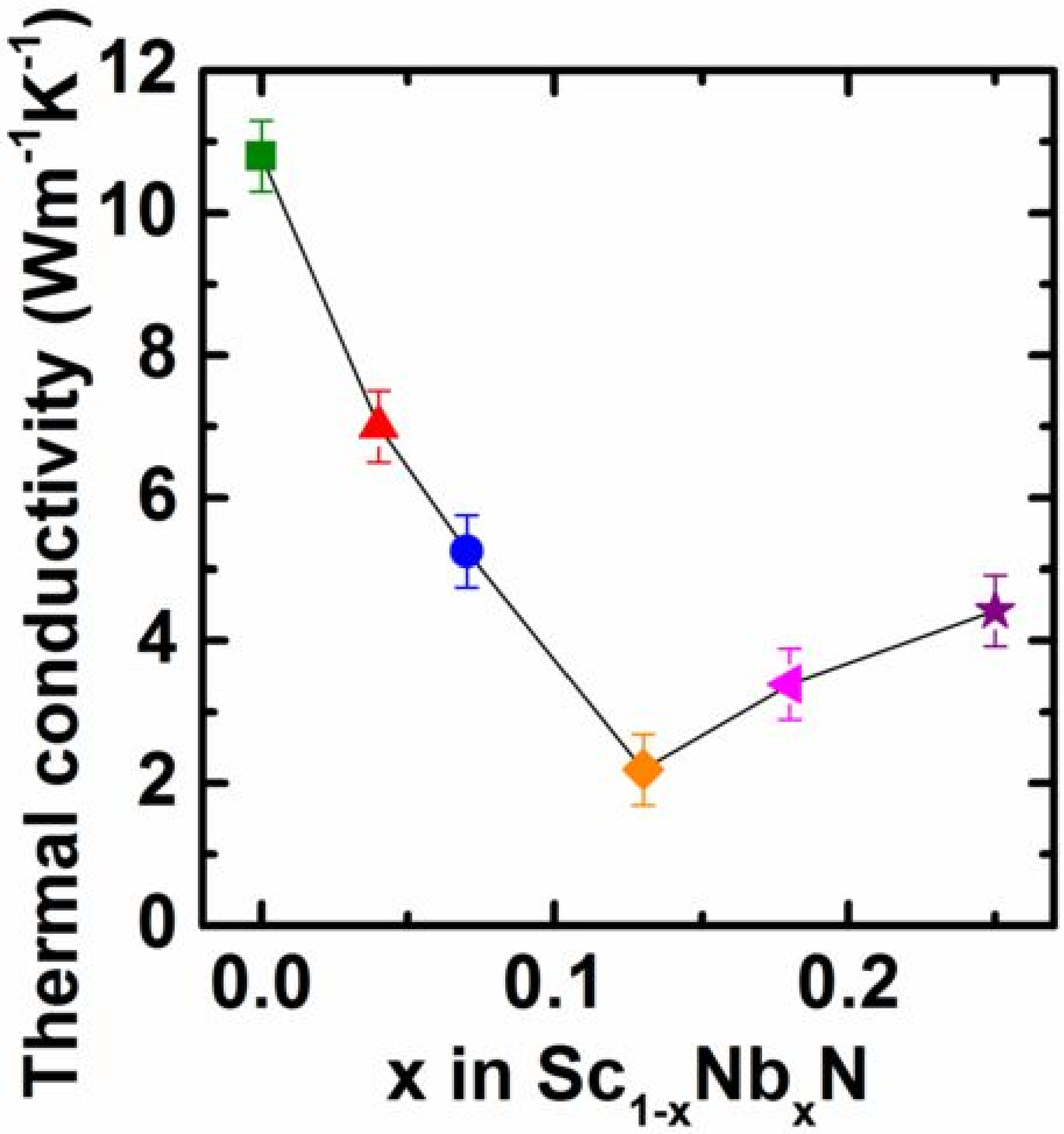
Thermal conductivity (Wm-1K-1)
0
2
4
6
8
10
12
0.0
0.1
0.2
x in Sc1-xNbxN

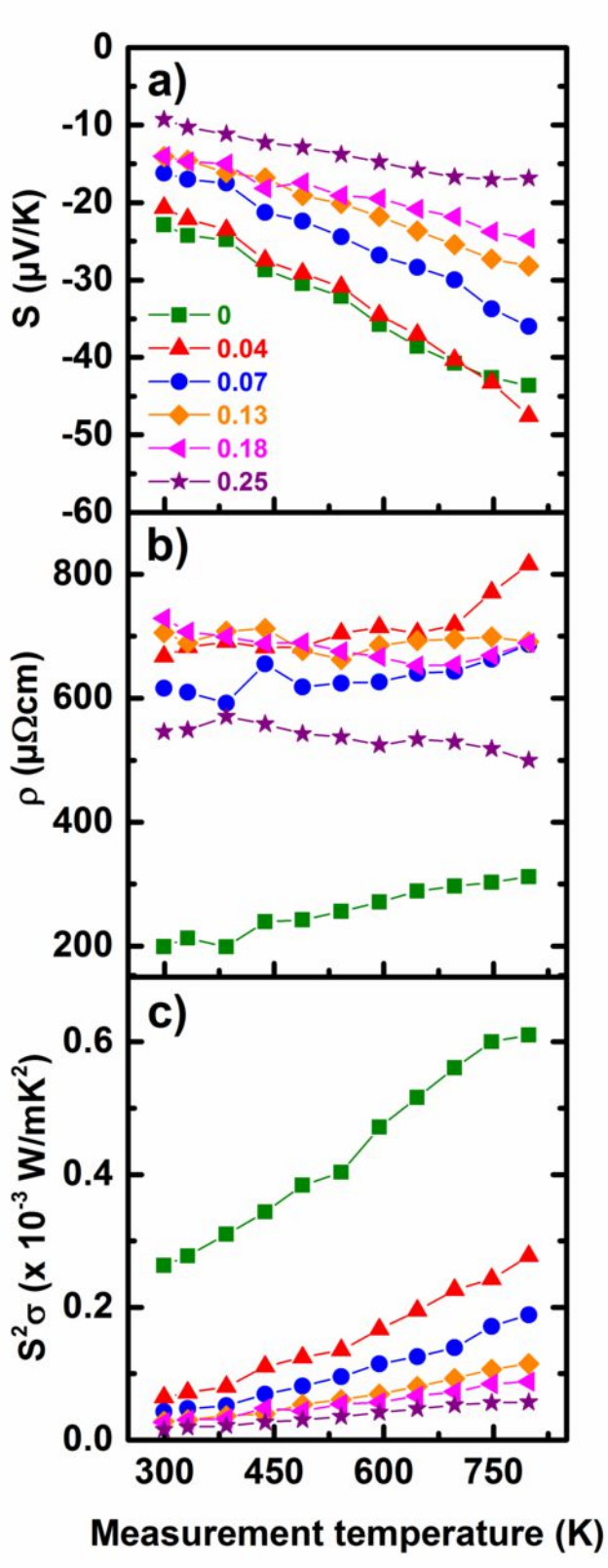
a)
b)
c)
S (μV/K)
ρ (μΩcm)
S²σ (x 10⁻³ W/mK²)
0
0.04
0.07
0.13
0.18
0.25
Measurement temperature (K)

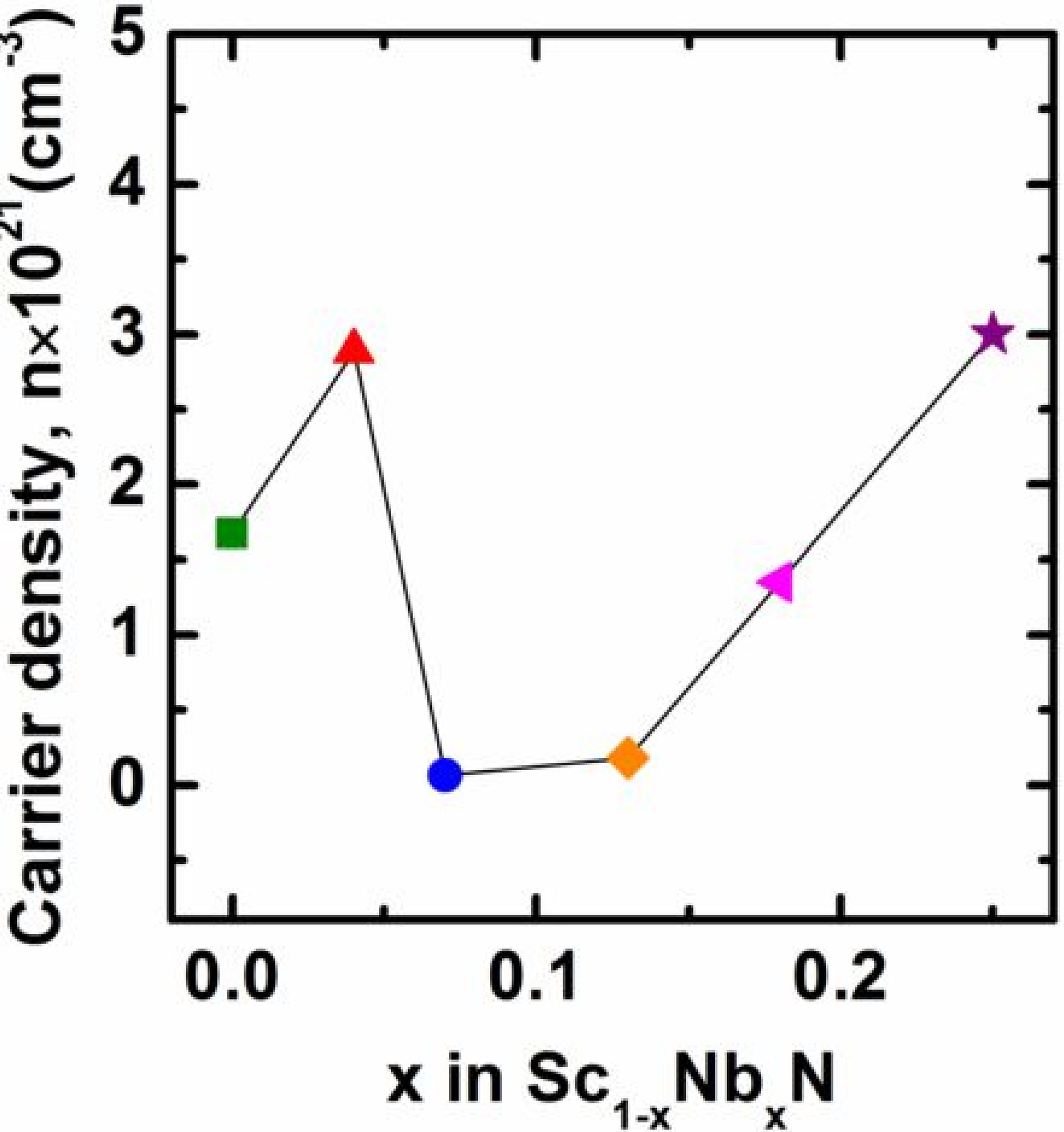
Carrier density, n×10^21 (cm^-3)
5
4
3
2
1
0
0.0
0.1
0.2
x in Sc1-xNbxN